Coiling and Folding: Buckling Instabilities of Viscous Fluid Jets

Sharmi Shah*
MIT Department of Mechanical Engineering

(18.3541: Nonlinear Dynamics: Continuum Systems)

(Dated: May 16, 2023)

The buckling of viscous fluid jets into coiling and folding patterns is an everyday phenomenon. The geometry of the orifice through which the fluid exits seems to play a significant role in whether the fluid coils or folds. The main parameter of interest was the critical dimensionless slit geometry at which the boundary between coiling and folding exists. A balancing argument between surface tension and gravitational effects was used to discover a relationship between slit geometry and other dimensionless parameters. This relationship was verified via dimensional analysis and experiment. Empirical results showed coiling occurs at low flow rates, greater heights, and low slit slendernesses and that the theorized curves for the critical dimensionless slit geometry are able to distinguish the trials during which the fluid coiled versus folded. More rigorous and comprehensive experimentation is required to validate any theoretical remarks made about the boundary between coiling and folding within this research.

Consider the simple act of pouring honey onto a stack of pancakes. As the honey flows from the bottle, it creates a distinctive pattern, forming a thin rope-like column that coils about itself. You may recall that in some instances, instead of coiling, this column will fold back and forth on itself. Both these folding and coiling behaviors are instabilities caused by fluid buckling - a phenomenon that many witness on the day to day. This everyday phenomenon has, in fact, been extensively studied over the last 60 years. Many researchers have created models to explain the relevant parameters that affect coiling and folding as well as the relative importance of these parameters [1]. For example, it has been determined that the frequency at which the fluid will coil has three different regimes (viscous, gravitational, inertial) and is dependent on parameters like flow rate and jet radius [2]. On the folding side, scaling analyses on the length and frequency scales of the folds have been conducted in conjunction with experiments to determine that similar parameters (flow rate and jet thickness) [3] govern folding behavior. Many papers have noted a less predictable stable boundary between coiling and folding [4]. As a result we look to answer the question of what determines whether a column of viscous fluid will coil or fold.

We can approach this question of folding versus coiling in fluid buckling by relating it to the more well-known field of buckling in solid mechanics (FIG. 1). The relevant parameters in solid buckling are material properties such as the Young's Modulus E and cross-sectional area moment of inertia I, as well as the length of the beam L. This means fluid properties, fluid column cross-section, and H (the height of the column) may be relevant parameters in our analysis. Furthermore, initial tests, performed by pouring honey into a cup, suggested that variables like flow rate (Q) and orifice (opening through which the fluid exits) geometry are important. Ultimately we define the relevant parameters as the height H from orifice to plate, acceleration due to gravity g , fluid flow rate Q, surface tension σ, density ρ, viscosity μ, orifice width t, orifice length d, and coiling/folding frequency ω.

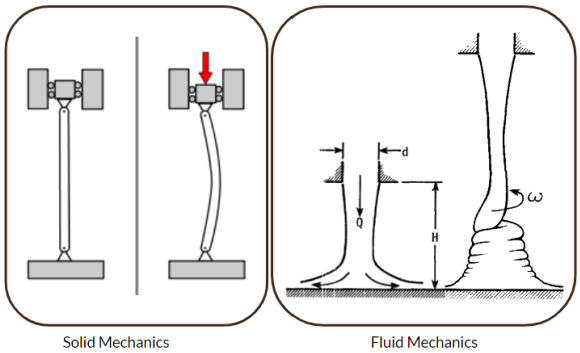

FIG. 1. Buckling of a slender beam in solid mechanics can be compared to the buckling of a slender, viscous jet in fluid mechanics. The jet will begin coiling or folding at the fluid interface if it is under enough compression. Several of the relevant parameters are labeled: d is the slit length, Q is the flow rate, H is the height, and ω is the coiling frequency.

We hypothesize that the boundary between coiling and folding is primarily controlled by the geometry of the stream at the fluid interface. One can imagine that the more circular the cross section of the column, the more likely the fluid is to coil. The geometry of the fluid column at at the fluid interface can then be seen as the limitation that either causes the buckling mode to be coiling or folding. If the stream tapers down enough from its orifice to the fluid interface, then the column may be of circular cross section. This indicates that the geometry of the orifice contributes to the geometry of the column at the fluid interface. Keeping this hypothesis in mind, we can formulate a set of dimensionless groups using the

* sharmis@mit.edu

Buckingham Pi Theorem and define the orifice geometry as a function of these groups:

$$\frac{d}{t} = f\left(\frac{\sigma}{\rho g H}, \frac{Q\mu}{\rho g H^4}, \omega\sqrt{\frac{H}{g}}, \frac{gH^3}{\nu^2}, \frac{d}{H}\right) \tag{1}$$

We then say that the "critical" orifice geometry, $\left(\frac{d}{t}\right)^*$, defines the boundary between coiling and folding and is a function of the non-dimensional groups seen in (1). We can neglect some of the non-dimensional groups, as some of them are not relevant to this critical orifice geometry. Below are the physical interpretations of all the pi groups:

$\frac{\sigma}{\rho g H^2}$ is the ratio of surface tension to gravitational forces,

$\frac{Q\mu}{\rho g H^4}$ is the ratio of viscous to gravitational forces,

$\omega\sqrt{\frac{H}{g}}$ is proportional to the square root of centrifugal acceleration to gravitational acceleration,

$\frac{gH^3}{\nu^2}$ is ratio of inertial to viscous forces, similar to a Reynold's number,

$\frac{d}{H}$ is a geometrical parameter relating slit length to stream height: "stream slenderness"

$\frac{d}{t}$ is a geometrical parameter relating slit length to slit width: "slit slenderness"

We can note that the first non-dimensional group listed is also equal to the square of the ratio of the capillary length, $\lambda_c = \sqrt{\frac{\sigma}{\rho g}}$, to the height of the stream. This is an intuitive way to compare the effects of surface tension and gravity.

According to [4], we can assume that the buckling process is a low-Reynold's-number phenomenon, implying that the term $\frac{gH^3}{\nu^2}$ can be neglected. Furthermore, experimental results suggest that, at the boundary between coiling and folding at any experimental point, the frequency does not change (i.e., coiling and folding occur at about the same frequency given a particular setup). As a result, the non-dimensional group $\omega\sqrt{\frac{H}{g}}$ may also be neglected. Hence, we obtain:

$$\left(\frac{d}{t}\right)^* = f\left(\frac{\sigma}{\rho g H^2}, \frac{Q\mu}{\rho g H^4}, \frac{d}{H}\right) \tag{2}$$

There is some critical slit slenderness ratio that defines the boundary between coiling and folding and it is a function of these 3 non-dimensional groups.

We can make a hypothesis for the dependencies of these dimensionless groups via a balance of surface tension and gravitational forces. The buckling phenomenon is an interplay between surface tension energy minimization that seeks to default to an axisymmetric stream and gravitational effects of a particle of fluid reaching a flat plate from an orifice. We can define a time constant for each of these effects: τ_g (gravitational time constant) and τ_s (surface tension time constant). When $\tau_g > \tau_s$, the surface tension effects act quickly, allowing the stream of fluid to taper into a circular cross-section before it reaches the interface, at which point it will likely coil. On the other hand, when $\tau_g < \tau_s$, the fluid reaches the interface before the surface tension effects transition the cross-section into a circle, resulting in a folding instability. To further this analysis, we define $\tau_s = \frac{d\mu}{\sigma}$ based on [5] and we can obtain $\tau_g = \frac{dtH}{Q}$ from dimensional analysis. At the boundary of coiling and folding, these effects balance, and thus we expect: $\tau_s \backsim \tau_g$. By rearranging terms from this relationship we can see that $\left(\frac{d}{t}\right)^* \backsim \frac{Hd\sigma}{Q\mu}$; we will term the latter expression the dimensionless gravitational time constant. This terminology is appropriate because the experiment varies $\frac{Hd\sigma}{Q\mu}$ only by varying those parameters which appear in τ_g (H, Q). This dimensionless gravitational time constant has a specific relationship with the non-dimensional groups we defined above, $\frac{Hd\sigma}{Q\mu} = \frac{\pi_1\pi_5}{\pi_2}$, resulting in:

$$\left(\frac{d}{t}\right)^* = \frac{\pi_1\pi_5}{\pi_2} \tag{3}$$

We now have a hypothesis for the functional dependence of the critical slit slenderness ratio on the relevant non-dimensional groups. In particular, we aim to experimentally verify the inverse relationship of $\left(\frac{d}{t}\right)^*$ on π_2 as well as the proportional relationship between $\left(\frac{d}{t}\right)^*$ and the dimensionless gravitational time constant, $\frac{Hd\sigma}{Q\mu}$, due to convenience of varying certain parts of the experimental setup.

The basic apparatus for the experiments is shown in FIG. 2 and consists of an orifice in a syringe through which a high-viscosity fluid is pushed with a plunger. The resulting stream falls onto a flat plate at a known distance H below the orifice. The orifice of the syringe contains an adjustable slit. Two rectangular parts can be slid back and forth and bolted down to adjust the slit length, d. The height, H, is controlled using a clamp which holds onto the syringe. The flow rate, Q, is controlled by pushing down on the plunger at different rates.

The two fluids used in the experiment were caramel and honey. The caramel and honey had viscosities of 15000 *cps* and 5000 *cps* respectively. The density of both fluids were estimated to be 1400 $\frac{kg}{m^3}$. Finally, the surface tension of the caramel was estimated as 80 $\frac{mN}{m}$ and sur-

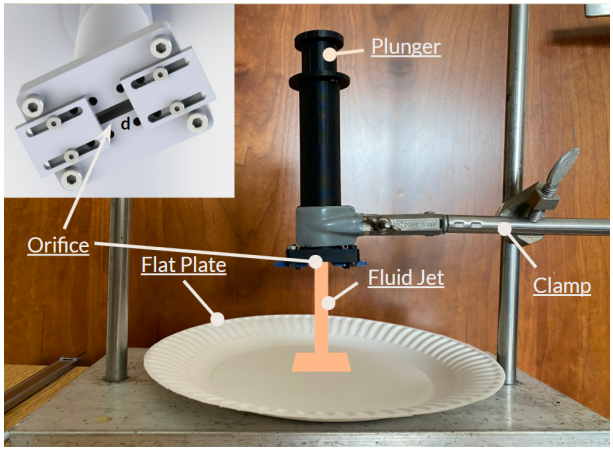

FIG. 2. Apparatus for experimental trials. The fluid is filled into the syringe and the plunger is used to extrude the fluid from the orifice onto the flat plate. The syringe has features to adjust the slit length while the clamp allows the control of the height, and the plunger allows control of flow rate.

face tension of honey was estimated as 55 $\frac{mN}{m}$. These parameters were obtained via several sources [6][7][8].

For each trial, a height was chosen, and the state of the fluid was recorded over a range of flow rates and slit geometries. Then the height would be increased and the flow rates and geometries would be varied again. This process was repeated for both fluids. The state of the fluid during each trial was organized into one of five categories: coiling, folding, stable, random, in-between. The stable state is characterized by the formation of a single smooth jet from the orifice to the flat plate. In the random state, no distinct pattern is visible and the fluid makes random patterns that neither resembled coiling nor folding. The in-between state is classified by the fluid folding at one instance and spontaneously coiling at the next. The in-between state was considered to be on the boundary of folding and coiling, where slight perturbations to the system made it swap between the two modes of buckling.

During the experiments some key observations were made. First, folding can be seen as a more stable version of the buckling instability. There were many instances when a fluid was coiling at a slow rate where increasing the flow rate resulted in folding and increasing it even further resulted in a stable jet. Second, more viscous fluids demonstrated a higher tendency to fold in general. Additionally, at small heights, coiling was not observed, even at low flow rates. For the more viscous fluid, coiling was only observed when the height was increased dramatically. Following experimentation, a number of plots were created to illustrate the functional relationships that were derived previously.

The experimental results were first plotted on a graph with the non-dimensional gravitational time constant on the x-axis and the slit slenderness ratio on the y-axis (Fig. 3). Each data point was also colored according to the fluid's observed state during the trial. According to the hypothesis that $\left(\frac{d}{t}\right)^* \backsim \frac{Hd\sigma}{Q\mu}$, one would expect a linear curve for the critical slit slenderness ratio, $\left(\frac{d}{t}\right)^*$, to separate the folding instability from the coiling on this plot. Therefore a linear curve was fitted to the observations that were in the in-between state - exactly at the boundary of coiling and folding. This line was plotted for both caramel and honey.

The results were also plotted on a graph with $\pi_2 = \frac{Q\mu}{\rho g H^4}$ on the x-axis and the slit slenderness ratio on the y-axis (Fig. 4). Once again, the data points were colored according to the fluid's observed state during the trial. As indicated functionally in (3), the slit slenderness is dependent on the dimensionless surface tension parameter, the dimensionless viscosity parameter, and the dimensionless height. Specifically, the relationship $\left(\frac{d}{t}\right)^* = \frac{\pi_1 \pi_5}{\pi_2}$ indicates that there is a physical interplay between surface tension and viscosity effects at the boundary of coiling and folding. This relationship also suggests that one would expect an inverse relationship for the curve in FIG. 4. As a result, a power law curve was fitted to the data points observed in the in-between state for both caramel and honey.

In both plots in FIG. 3 the coiling observations are congregated to the bottom left. (More coiling observations could exist on the right side of the plot, but they did not in this research due to limitations in the breadth of experimental trials performed). This makes sense because a low slit slenderness ratio will reduce the time needed for the surface tension to taper the slit geometry into a circle at a certain height. It is presumed that the folding observations are clustered at greater values of the slit slenderness ratio for the opposite reason. More observations were recorded than the ones shown in FIG.3 but were left out for ease of visualizing the most dense part of the plots. However, the excluded observations also followed the same pattern stated above.

For the plots in FIG. 3 the line of best fit splits the graph into two sections. We see that points below the line are mostly observed in a state of coiling or a random state whereas the points above the line are observed to be folding or stable. 98% of the data points for caramel and 92% of the data points for honey are classified correctly with the respective lines of best fit. This bisection follows the theory which predicted that a linear curve would divide the observations of coiling and folding. There is a difference in the slope of the line between the two plots, with the lower viscosity fluid, honey, having a greater sloped line. It is postulated that the two fluids may be in different regimes of critical slit slenderness ratio due to the magnitudes of difference in their viscosities.

Some general observations can also be made based on the plots shown in FIG. 4. Once again, coiling is clustered at the bottom left of the graph. The small slit slenderness ratio predictably plays a role in the coiling observations

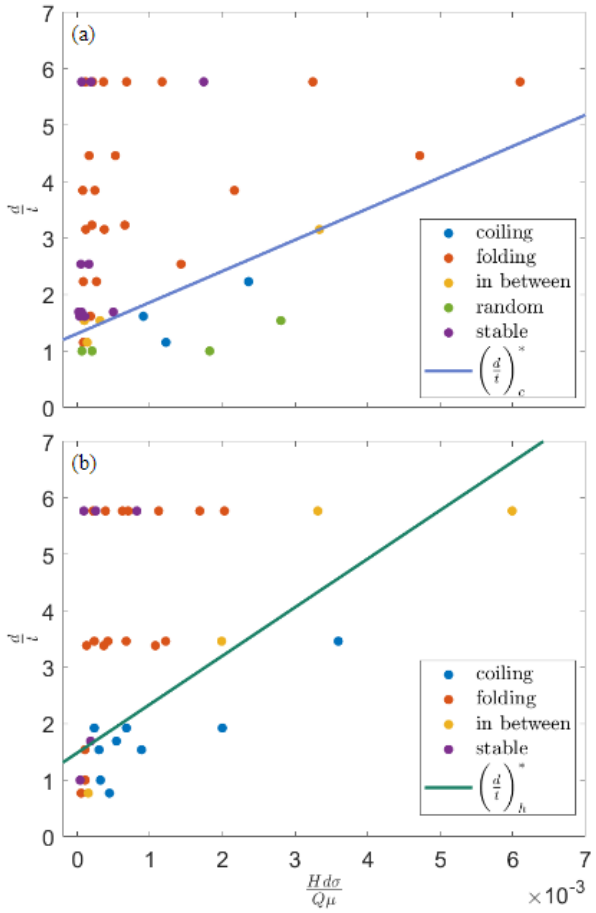

FIG. 3. Dimensionless gravitational time constant and slit slenderness values were calculated for each data point for both fluids: (a) caramel and (b) honey. Each point was also labeled corresponding to the observed state of the fluid during that trial. A curve of form $ax + b$ was fitted to the points in the in-between state for both fluids. The blue curve in (a) had values $a = 553$, $b = 1.31$ and correctly separated 98% of the data points. The green curve in (b) had values $a = 859$, $b = 1.48$ and correctly separated 92% of the data points. The difference in slope may be a result of significant differences in viscosities between the two fluids, potentially resulting in different regimes of buckling instabilities.

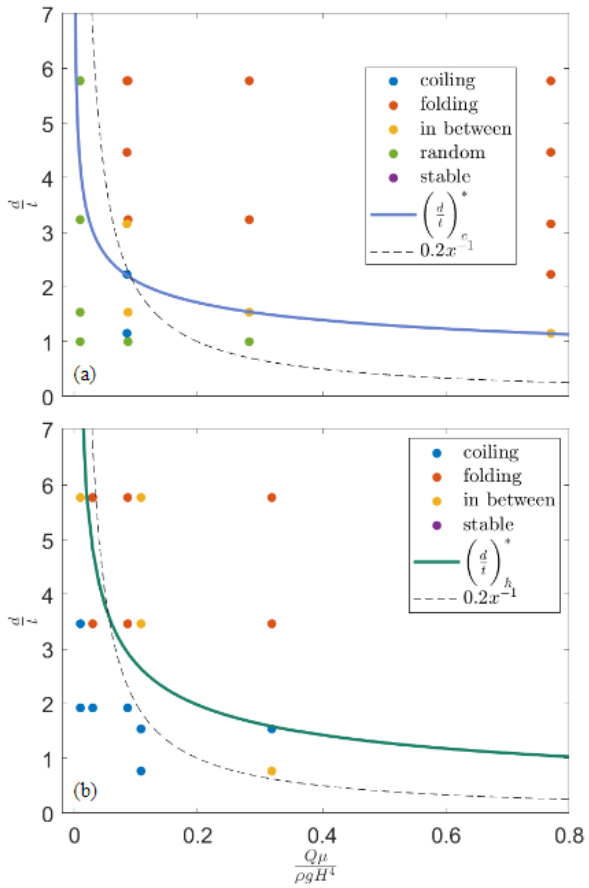

FIG. 4. Dimensionless viscosity and slit slenderness values were calculated for each data point for both fluids: (a) caramel and (b) honey. Each point was also labeled corresponding to the observed state of the fluid during that trial. A curve of form bx^m was fitted to the points in the in-between state for both fluids. The blue curve in (a) had values $b = 1.06$ and $m = -0.299$ and correctly separated 98% of the data points. The green curve in (b) had values $b = 0.929$ and $m = -0.470$ and correctly separated 86% of the data points. Neither of these curves represent a true inverse relationship that was theorized by the earlier dimensional analysis. A black dotted line is plotted for reference in both graphs as an example curve for an inverse relationship.

occurring towards the bottom of the plot. Coiling is also more likely to occur at low flow rates and greater heights, explaining the aggregation of coiling observations on the left of the plot. This is once again attributed to the interplay between surface tension and gravitational forces. If the flow rate is small or the height is large, the fluid has more time to reach the fluid interface and transition into a cylindrical jet. On the other hand, a greater flow rate will push the fluid quickly such that in many instances it will fold at the fluid interface. In fact, out of all the trials tested at three different flow rates, only one trial resulted in coiling behavior at the fastest flow rate.

The fitted power law curves in FIG. 4 indicate that such a curve does split the data in the two desired groups. In both plots the coiling and random observations are below the curve where the surface tension time constant is greater, whereas the folding and stable observations are above the curve. While the critical slenderness ratio curves for caramel and honey classify 98% and 86% of the data correctly, respectively, these curves are not exactly the expected inverse relationships. This is likely due to the limitations in sample sizes as well as accuracy in measurements of both fluid parameters and flow parameters like Q. An example curve with a true inverse relationship is plotted in these graphs as a black dotted line, suggesting that an inverse relationship can categorize the data similarly, but may just require more sample

points.

In conclusion, we have determined which parameters affect the buckling instabilities seen commonly in viscous fluids. Theory suggests that whether a fluid folds or coils depends on the balance of surface tension and gravitational effects. This "time-scale" analysis agrees with the formation of dimensionless groups from Buckingham Pi analysis. The experiments generally validate the derived functional dependencies. First, the critical slit slenderness ratio (coiling versus folding boundary) is positively correlated with the non-dimensional gravitational time constant. Second, the critical slit slenderness displays an inverse relationship with the dimensionless viscosity. With more controlled experimentation, more fluids, and many more sample points this experimentation could be furthered greatly to add to our knowledge about the boundary between these two phenomena.

[1] N. M. Ribe, Coiling of viscous jets, Proc. R. Soc. Lond. A. **460**, 3223–3239 (2004).

[2] M. H. N. M. Ribe and D. Bonn, Stability of liquid rope coiling, Physics of Fluids **18**, 268 (2006).

[3] M. Skorobogatiy and L. Mahadevan, Folding of viscous sheets and filaments, Europhysics Letters **812**, 532–538 (2000).

[4] J. O. Cruickshank and B. R. Munson, Viscous fluid buckling of plane and axisymmetric jets, Journal of Fluid Mechanics **113**, 221 (1981).

[5] H. A. Stone and L. G. Leal, Relaxation and breakup of an initially extended drop in an otherwise quiescent fluid, Journal of Fluid Mechanics **198**, 339 (1989).

[6] Global Pumps, List of typical viscosities (2023).

[7] Aqua Calc, (2023).

[8] Culinary Nutrition, High fructose corn syrup (2013).

[9] M. H. N. M. Ribe and D. Bonn, Liquid rope coiling, Journal of Fluid Mechanics **812** (2017).

Coiling and Folding Buckling Instabilities of Viscous Fluid Jets: Supplement

Sharmi Shah*
MIT Department of Mechanical Engineering

(18.3541: Nonlinear Dynamics: Continuum Systems)

(Dated: May 16, 2023)

I. BUCKINGHAM PI

The Buckingham Pi Theorem was used to non-dimensionalize the relevant parameters. This supplement shows the details that were not shown in the report.

$0 = f(H, g, Q, \sigma, \rho, \mu, t, \omega, d)$

There were 3 units used so j=3. We can use ρ, g, and H as the 3 parameters to non-dimensionalize all of the remaining parameters as they themselves do not form a non-dimensional group.

H	g	Q	σ	ρ	μ	t	f	d
L	$\frac{L}{T^2}$	$\frac{L^3}{T}$	$\frac{M}{T^2}$	$\frac{M}{L^3}$	$\frac{M}{LT}$	L	$\frac{1}{T}$	L

Pi-Group 1:

$[\sigma] = \frac{M}{T^2}$

$\frac{M}{T^2}\frac{L^3}{M}\frac{T^2}{L}\frac{1}{L^2} = 1$

$\sigma\frac{1}{\rho}\frac{1}{g}\frac{1}{H^2} = 1 \rightarrow \pi_1 = \frac{\sigma}{\rho g H^2}$

Pi-Group 2:

Using just Q, g, and H results in a non-dimensional group $\frac{Q}{\sqrt{gH^5}}$. However this group isn't a very physically intuitive pi-group and so we use the analysis below:

$[Q] = \frac{L^3}{T}$

$\frac{L^3}{T}\frac{T^2}{L}\frac{L^3}{M}\frac{M}{LT}\frac{1}{L^4} = 1$

$Q\frac{1}{g}\frac{1}{\rho}\mu\frac{1}{H^4} \rightarrow \pi_2 = \frac{Q\mu}{g\rho H^4}$

This group represents a ratio between viscous and gravitational forces.

Pi-Group 3:

$[f] = \frac{1}{T}$

$\frac{1}{T}\left(\frac{T^2}{L}\right)^{0.5} L^{0.5} = 1$

$f\frac{1}{\sqrt{g}}\sqrt{H} \rightarrow \pi_3 = f\sqrt{\frac{H}{g}}$

This group is proportional to the square root of the ratio between centrifugal acceleration and gravitational acceleration.

Pi-Group 4:

$[\mu] = \frac{M}{LT}$

$\frac{M}{LT}\frac{L^3}{M}\left(\frac{T^2}{L}\right)^{0.5}\left(\frac{1}{L}\right)^{1.5} = 1$

$\mu\frac{1}{\rho}\frac{1}{\sqrt{g}}\frac{1}{H^{1.5}} = \sqrt{\frac{\mu^2}{\rho^2 g H^3}}$

We square this group for cleanliness and substitute in ν:

$\frac{\nu^2}{gH^3}$

This non-dimensional group is like a Reynold's number because it's a ratio describing the inertial to viscous terms in the system. To be consistent with the Reynold's number, we flip the pi-group to get:

$\pi_4 = \frac{gH^3}{\nu^2}$

Pi-Group 5:

This group is trivial to derive. It represents the slenderness of the stream.

$[H] = L$

$\pi_5 = \frac{d}{H}$

Pi-Group 6:

This group is also trivial to derive. It represents the slenderness of the slit or the aspect ratio of the orifice.

$[H] = L$

$\pi_6 = \frac{d}{t}$

II. TIME CONSTANTS

$\tau_g = \frac{H}{u} = \frac{H}{\frac{Q}{dt}} = \frac{Hdt}{Q}$

$\tau_s = \frac{d\mu}{\sigma}$

$\tau_g \backsim \tau_s \rightarrow \frac{Hdt}{Q} \backsim \frac{d\mu}{\sigma} \rightarrow \left(\frac{d}{t}\right)^* \backsim \frac{Hd\sigma}{Q\mu}$

* sharmis@mit.edu

The interplay between the surface tension and gravitational time constants that was stated in the article used the above analysis. The gravitational time constant was defined as the height the fluid was falling across divided by the velocity. The velocity could then be written as a ratio of the flow rate to orifice cross-section, dt which resulted in the final form. As mentioned in the article, the surface tension time constant was taken from a paper by Stone and Leal. We know that at the boundary of coiling and folding the time constants will balance each other and have similar magnitudes. From this we can rearrange the variables to acquire the critical slit slenderness in terms of other parameters.

III. ADDITIONAL FIGURES

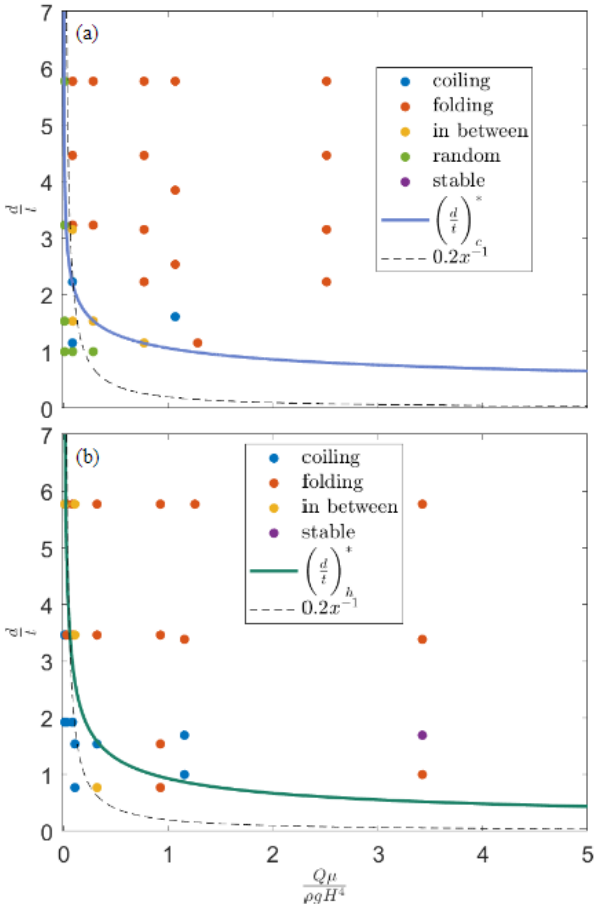

FIG. 1. These graphs show a wider range of the data that was on the plots that are shown in FIG. 4 in the article. They show a couple of the points that were incorrectly classified, as well as the trend of folding occurring at high flow rates and low heights. (a) represents the plot with the caramel trials and (b) represents the plot with the honey trials.